Supplementary Information for

Engineering multi-layered yolk-shell $CuO@Cu_xSn_{1-x}O_2$ (x=0, 0.1, 0.2, and 0.3) heterojunction for photocatalytic H_2 generation from atmospheric moisture

Farzad Hasanvandian[a], Hesam Akbari[a], Amir Adibzadeh[a,b], Babak Kakavandi[c], Hamed Akbari[a,]*

[a] *Health Research Center, Lifestyle Institute, Baqiyatallah University of Medical Sciences, Tehran, Iran*

[b] *Department of Environmental Health Engineering, Faculty of Health, Baqiyatallah University of Medical Sciences, Tehran, Iran*

[c] *Department of Environmental Health Engineering, Alborz University of Medical Sciences, Karaj, Iran*

1. Experimental

[*] Corresponding authors: Health Research Center, Lifestyle Institute, Baqiyatallah University of Medical Sciences, Tehran, Iran (Hamed Akbari)

E-mail addresses: Akbarihamed_2005@yahoo.com

1.1. Chemical and agents

All chemicals and solvents were obtained from Merck (Darmstadt, Germany) and employed directly without any further purification steps. Tin(II) chloride dihydrate ($SnCl_2 \cdot 2H_2O$) and copper(II) nitrate trihydrate ($Cu(NO_3)_2 \cdot 3H_2O$) served as the metal precursors for Sn and Cu, respectively. The solvents applied in this work consisted of isopropanol (C_3H_8O), glycerol ($C_3H_8O_3$), and ethanol (C_2H_6O). The pH of the reaction media was regulated using sodium hydroxide (NaOH) and hydrochloric acid (HCl, 37%). Throughout all experimental procedures, deionized (DI) water was utilized.

1.2. Nanostructure characterization method

The crystallographic features of the synthesized photocatalysts were analyzed using X-ray diffraction (XRD) with a PANalytical X'Pert Pro MPD diffractometer (Netherlands), operated under Cu Kα radiation (λ = 0.15406 nm) at 40 kV and 30 mA. Morphological characteristics were investigated via field-emission scanning electron microscopy (FE-SEM, Mira III, Tescan, Czech Republic) and transmission electron microscopy (TEM, CM300, PHILIPS, Netherlands). The elemental oxidation states and electronic interactions were determined through X-ray photoelectron spectroscopy (XPS) employing a K-Alpha spectrometer (Bes Tec, Germany) with Mg Kα radiation (excitation energy = 1253.6 eV). Textural parameters such as surface area and pore distribution were obtained through nitrogen adsorption–desorption analysis on a BELSORP MINI II system (BEL, Japan). Optical absorption and light-harvesting behaviors were recorded using UV–Vis diffuse reflectance spectroscopy (DRS, Avaspec-2048-TEC, Avantes, Netherlands). Photoluminescence (PL) spectra, collected with a Cary Eclipse spectrofluorometer (Agilent, USA), provided insight into charge carrier recombination dynamics.

Photoelectrochemical performance was examined using transient photocurrent (TPC), electrochemical impedance spectroscopy (EIS), and Mott–Schottky (MS) analyses on a PGSTAT302N potentiostat in a

conventional three-electrode configuration. The working electrode was a catalyst-coated glassy carbon electrode (C-GCE), the counter electrode was a platinum wire, and Ag/AgCl served as the reference electrode in a 0.5 M Na_2SO_4 electrolyte. EIS spectra were acquired under open-circuit potential conditions with a 10 mV AC oscillation over a frequency range of 100 kHz–0.01 Hz, while MS curves were recorded at fixed frequencies of 0.5, 1, and 1.5 kHz. For TPC tests, a catalyst-coated fluorine-doped tin oxide (C-FTO) electrode was subjected to intermittent illumination using a 300 W Xe lamp with 50 s on/off cycles. Detailed electrode preparation procedures for GCE and FTO substrates can be found in previous reports [1].

2. calculations

2.1. Scherrer formula

$$D = \frac{K \times \lambda}{\beta \times \cos(\theta)} \tag{S1}$$

where, D: crystalline size (nm), K: Shape factor, λ: wavelength of the X-ray, β: width of the diffraction peak, θ: diffraction angle,

2.2. The bi-exponential function of time-resolved PL

$$I(t) = A_1 \exp(-\frac{t}{T_1}) + A_2 \exp(-\frac{t}{T_2}) \tag{S2}$$

$$\text{long-lifespan decay} = \frac{A_2 T_2}{A_1 T_1 + A_2 T_2} \tag{S3}$$

$$\tau_{ave.} = \frac{A_1 T_1^2 + A_2 T_2^2}{A_1 T_1 + A_2 T_2} \tag{S4}$$

2.2.1. Fabrication of $Cu_xSn_{1-x}O_2$(x=0, 0.1, 0.2, and 0.3)

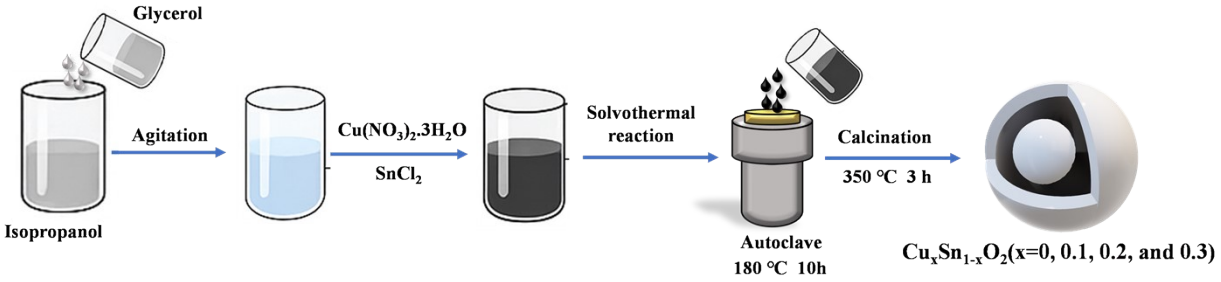

2.2.2. Fabrication of CuO

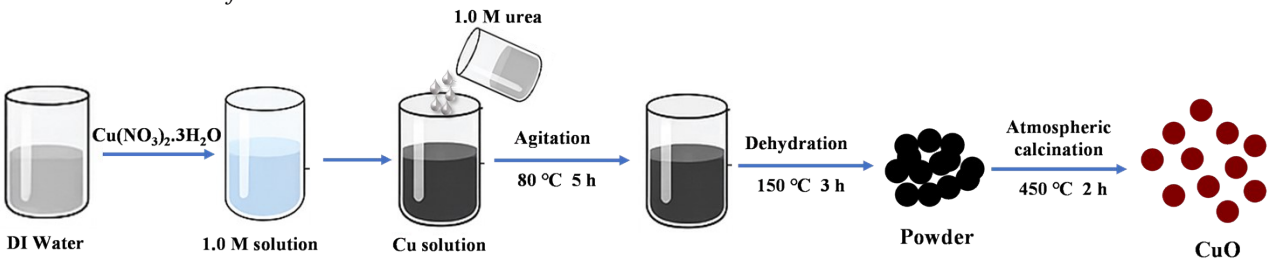

2.2.3. Fabrication of CuO@$Cu_xSn_{1-x}O_2$(x=0, 0.1, 0.2, and 0.3)

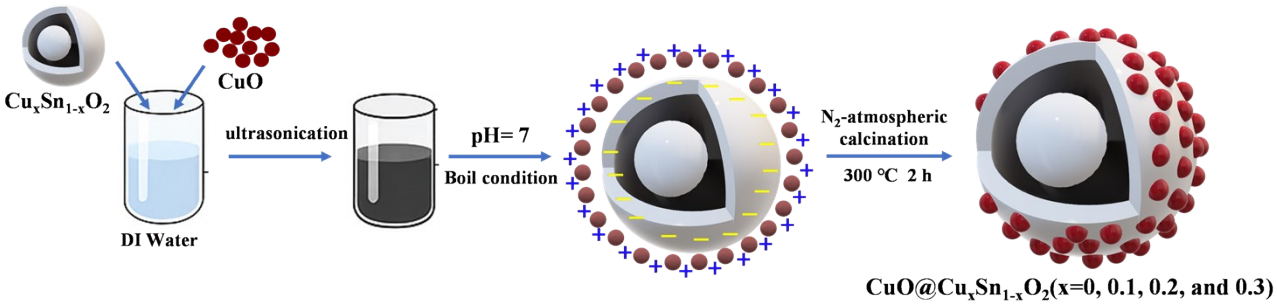

Fig. S1. The graphical presentation of synthesis procedure of catalysts.

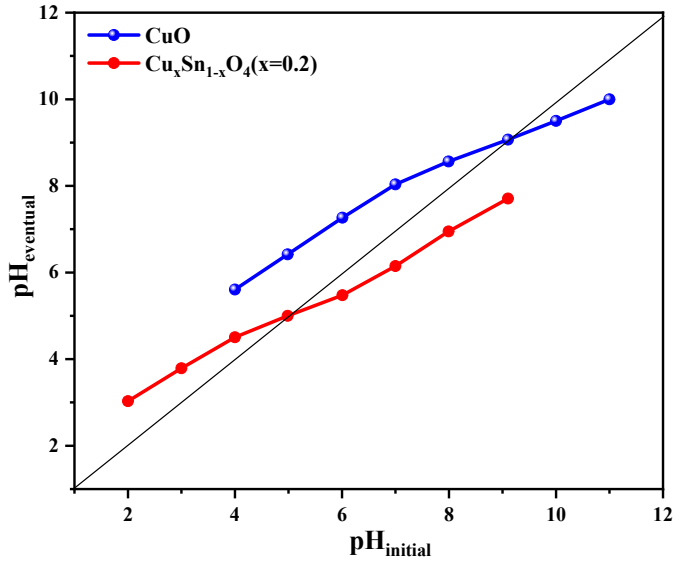

Fig. S2. Determination of pH_{ZPC} for CuO and $Cu_xSn_{1-x}O_4$(x=0.2) samples.

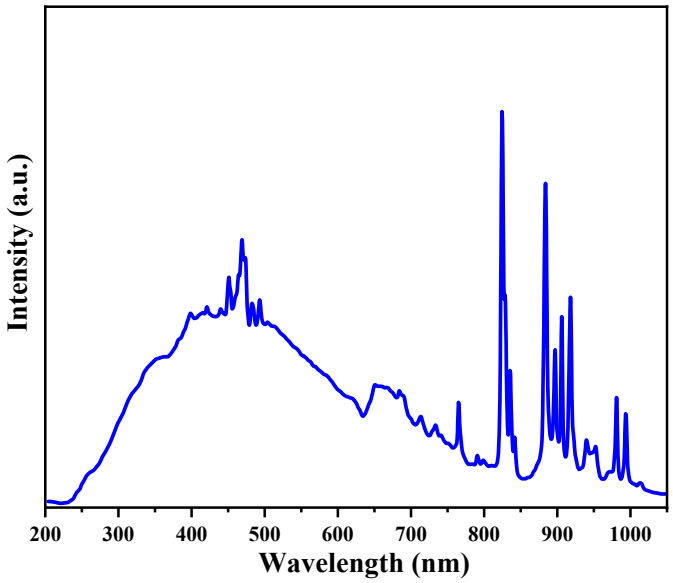

Fig. S3. The spectrum of Xe lamp.

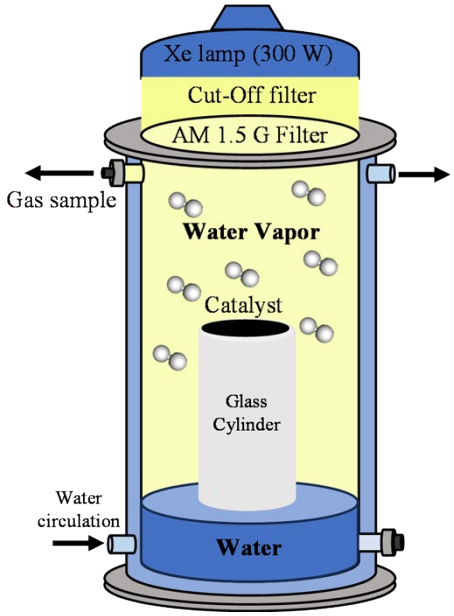

Fig. S4. Graphical presentation of atmospheric water splitting setup.

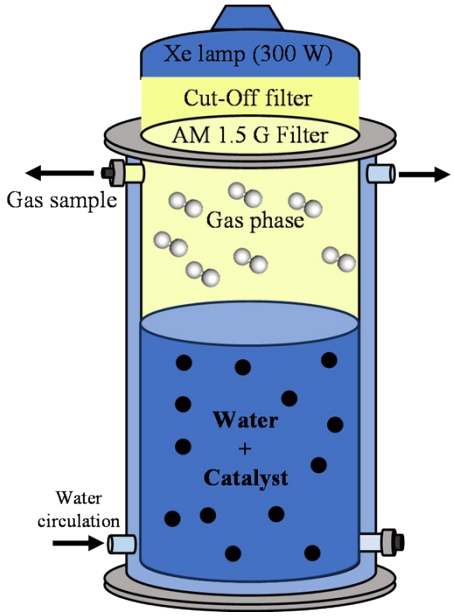

Fig. S5. Graphical presentation of conventional liquid-phase water splitting setup.

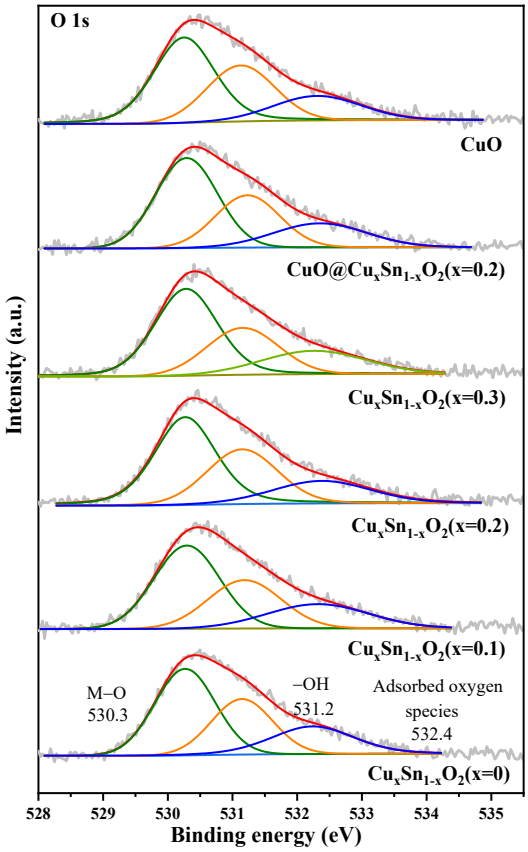

Fig. S6. HR-XPS patterns of O 1s related to various as-synthesized nanomaterials.

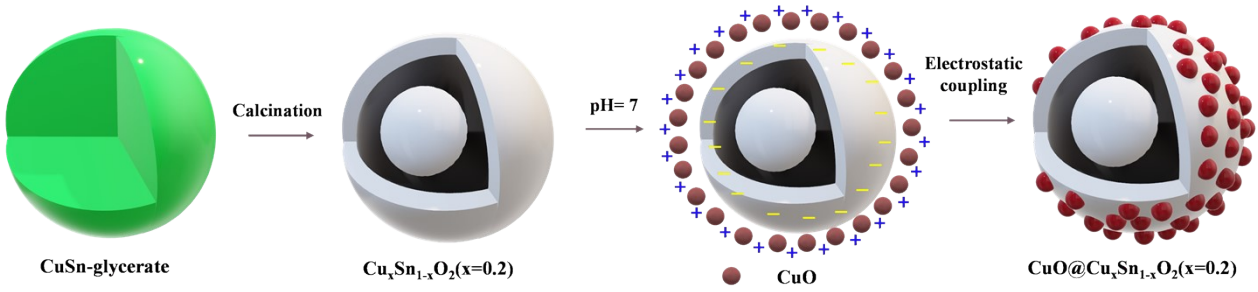

Fig. S7. Schematical illustration of the stepwise synthesis of multi-layered CuO@$Cu_xSn_{1-x}O_2$(x=0.2) yolk-shell hollow sphere.

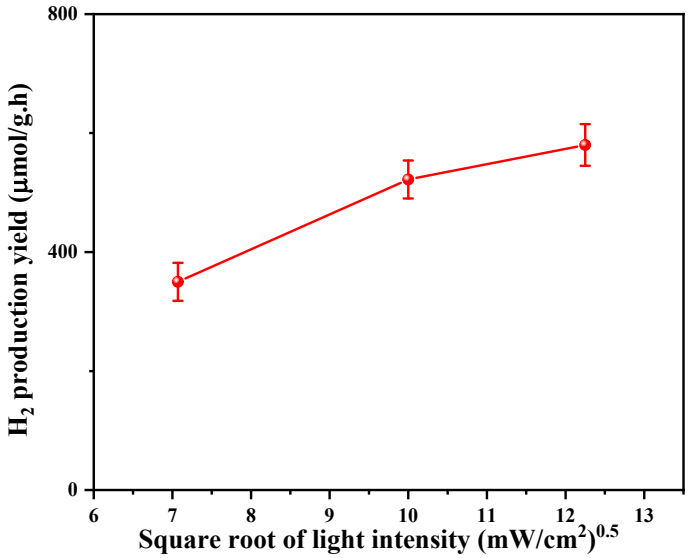

Fig. S8. Effect of the light intensity on the H_2 production performance of optimal CuO@$Cu_xSn_{1-x}O_2$(x=0.2).

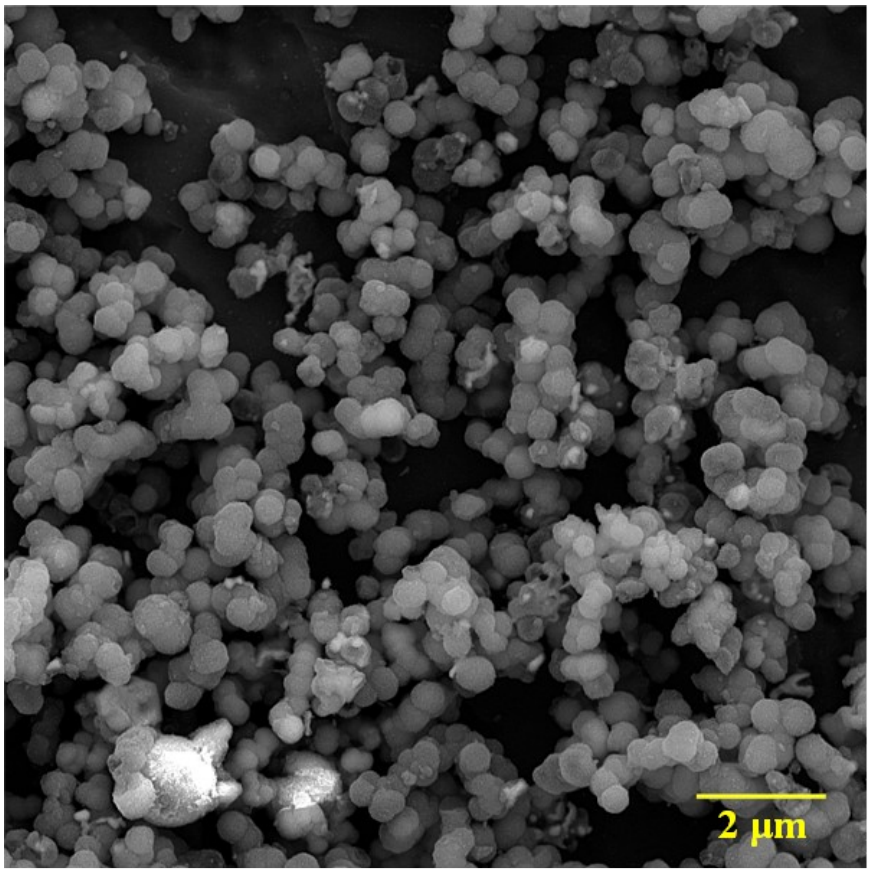

Fig. S9. The FE-SEM of CuO@$Cu_xSn_{1-x}O_2$(x=0.2) nanocomposite after ten repetitive cycles of PAMS reaction

Table S1. The extracted parameters for time-resolved PL singles.

Sample	T_1	A_1	T_2	A_2	long-lived carrier percentage (%)	$T_{ave.}$ (ns)
$Cu_xSn_{1-x}O_2$(x=0)	1.5	15	2.4	19	67	2.12
$Cu_xSn_{1-x}O_2$(x=0.1)	1.7	15	3.7	21	75	3.21
$Cu_xSn_{1-x}O_2$(x=0.2)	1.9	16	4.8	26	80	4.23
$Cu_xSn_{1-x}O_2$(x=0.3)	1.8	16	4.1	25	76	3.60
CuO	1.5	13	1.2	12	29	1.37
CuO@$Cu_xSn_{1-x}O_2$(x=0.2)	2.9	22	12	31	85	10.66

Table. S2. comparison study between the catalytic activity of optimized CuO@$Cu_xSn_{1-x}O_2$(x=0.2) and recently reported nanomaterials for PAMS system.

Sample	Catalyst form	Light Source	Sacrificial agents	Reaction conditions	PAMS efficiency	Ref.
MOF-801-hydrazine-$SrTiO_3$:Al	Powder	300 W Xe	-	30% RH, 25°C	1033.10 μmol/g.h	[2]
Al-doped $SrTiO_3$ loaded with a $RhCrO_x$ and CoO_y	Coated layer	300 W Xe	-	58% RH, 30°C	0.677 μmol/h cm^2	[3]
NFC@LiCl-SrTiO3:Al	Block gel	300 W Xe	-	90% RH, 25°C	6.80 μmol/h cm^2	[4]
carbonized wood/$ZnCl_2$/Pt@g-C_3N_4	Coated layer	300 W Xe	-	70% RH, 25°C	4.0 μmol/h cm^2	[5]
$CaC1_2$-PAAm-Pt-TiO_2/PTFE	Block	300 W Xe	Polyethylene Glycol	75% RH, 28°C	425 μmol/g.h	[6]
photosensitive pyrene COF (Py-HMPA@Pt)	Coated layer	300 W Xe (λ≥420 nm)	Ascorbic Acid	48% RH, 28°C	105 μmol/g.h	[7]
RhCrO*x*–Al:SrTiO3	Coated layer	Solar Simulator (AM 1.5G)	-	25°C	2.6 μmol/h cm^2	[8]
CuO@$Cu_xSn_{1-x}O_2$(x=0.2)	**Coated layer**	**300W Xe (λ≥420 nm)**	**Ascorbic Acid**	**48% RH, 28°C**	**1332 μmol/g.h (8.48** μmol/h cm^2)	**This study**
		Solar Simulator			**733 μmol/g.h (4.67** μmol/h cm^2)	

		AM 1.5G filter (100 mW/cm^2)				

Table S3. comparison study between the catalytic activity of optimized CuO@$Cu_xSn_{1-x}O_2$(x=0.2) and recently reported nanomaterials for conventional liquid-phase H_2 production.

Sample	**Light Source**	**Sacrificial or Co-Catalyst agents**	**STH (%)**	**AQE (%)**	**H_2 production yield (μmol/g.h)**	**Ref.**
2D/2D β-NiS/TiO_{2-x}	300 W Xe (λ≥380 nm)	-	0.44	9.13	380	[9]
$CdS_{h/l}$-2	300 W Xe (λ≥420 nm)	-	-	10.08 (at 420 nm)	3200	[10]
	Solar Simulator AM 1.5G filter		0.94	-	1066	
PMA_2PbI_4/MoS_2	300W Xe AM 1.5G filter (150 mW/cm^2)	HI solution (1.25 mol/L)	2.31	12.32 (at 400 nm)	736.6	[11]
g-C_3N_4/rGO/PDIP	300 W Xe (λ≥420 nm)	Pt/Cr_2O_3 $Co(OH)_2$ (co-catalysts)	-	4.94 (at 420 nm)	316	[12]
	Solar Simulator AM 1.5G filter		0.3	-	92.2	
Ir(P.I.)/BVO-573	300 W Xe (λ≥420 nm)	K3[Fe(CN)$_6$] (5 mM) Buffer Solution ZrO_2/TaON (150 mg)	-	16.9 (at 420 nm)	4000	[13]
	Solar Simulator AM 1.5G filter		0.9	-	1916	
Au/CoOx-BiVO4	300 W Xe (λ≥420 nm)	K3[Fe(CN)6] (10 mM) buffer solution $RhyCr_2–yO_3$-ZrO_2/TaON (50 mg)	-	10.3 (at 420 nm)	2600	[14]
	Solar Simulator AM 1.5G filter		0.5	-	600	
$Ta_3N_5/KTaO_3$	300 W Xe (λ≥420 nm)	Rh/Cr_2O_3 (co-catalyst)	-	0.22 (at 420 nm)	36.7	[15]
	Solar simulator (AM 1.5 G)		0.014	-	22	
MgTa2O6−xNy/TaON	300 W Xe (λ≥420 nm)	Na_3RhCl_6 K_2CrO_4	-	12.3 (at 420 nm)	800	[16]
	Solar Simulator		0.6	-	180	

	AM 1.5G filter (100 mW/cm^2)					
Ni-TBAPy-NB	300 W Xe (λ≥420 nm)	ascorbic acid (15 mM) MeOH (90 mL)	-	8.0 (at 420 nm)	5000	[17]
MoSe2/FPBI	Solar simulator (AM 1.5 G)	HBr/HI acid solutions	-	30.66 (at 420 nm)	8550	[18]
Graphene/ZnO/CuO	300 W Xe (λ≥420 nm)	TEOA	-	-	37200	[19]
CuO@$Cu_xSn_{1-x}O_2$(x=0.2)	**300W Xe (λ≥420 nm)**	**Ascorbic Acid**	**-**	**8.2 (at 420 nm)**	**16820**	**This study**
	Solar simulator AM 1.5G filter (100 mW/cm^2)		**0.47**	**-**	**5942**	

References

[1] F. Hasanvandian, M.Z. Salmasi, M. Moradi, S.F. Saei, B. Kakavandi, S.R. Setayesh, Enhanced spatially coupling heterojunction assembled from CuCo2S4 yolk-shell hollow sphere capsulated by Bi-modified TiO2 for highly efficient CO2 photoreduction, Chem. Eng. J. 444 (2022) 136493.

[2] X. Yan, L. Tian, J. Huang, X. Zhao, F. Liu, R. Zhao, X. Guan, J. Shi, W. Chen, M. Liu, Integrated System for Photocatalytic Overall Water Splitting from Arid Air, Nano Lett. 25 (2024) 71–76.

[3] C.J. Shearer, T. Hisatomi, K. Domen, G.F. Metha, Gas phase photocatalytic water splitting of moisture in ambient air: Toward reagent-free hydrogen production, J. Photochem. Photobiol. A Chem. 401 (2020) 112757.

[4] X. Yan, L. Tian, F. Xue, J. Huang, R. Zhao, X. Guan, J. Shi, W. Chen, M. Liu, In situ hydrogen production in all-level-humidity air: integrating atmospheric water harvesting with photocatalysis, EES Catal. (2025).

[5] L. He, X. Zeng, H. Chen, L. Zhao, Z. Huang, D. Wang, X. He, W. Fang, X. Du, W. Li, A hybrid photocatalytic system splits atmospheric water to produce hydrogen, Adv. Funct. Mater. 34 (2024) 2313058.

[6] L. Huang, P. Liu, C. Qin, C. Gui, X. Zhang, T. Ren, Y. Ge, Y. Yu, Z. Liu, L. Chen, Solar-driven hydrogen production based on moisture adsorption-desorption cycle, Nano Energy. 128 (2024) 109879.

[7] Y. Liu, W.-K. Han, W. Chi, J.-X. Fu, Y. Mao, X. Yan, J.-X. Shao, Y. Jiang, Z.-G. Gu, One-dimensional covalent organic frameworks with atmospheric water harvesting for photocatalytic hydrogen evolution from water vapor, Appl. Catal. B Environ. 338 (2023) 123074.

[8] C. Pornrungroj, A. Bin Mohamad Annuar, Q. Wang, M. Rahaman, S. Bhattacharjee, V. Andrei, E. Reisner, Hybrid photothermal–photocatalyst sheets for solar-driven overall water splitting coupled to water purification, Nat. Water. 1 (2023) 952–960.

[9] J. Liu, Y. Wan, Y. Xie, F. Dong, K. Yang, X. Li, Boosting photocatalytic overall water splitting by β-NiS/TiO2-x Ohmic junction, Appl. Catal. B Environ. Energy. (2025) 125690.

[10] J. Wang, Y. Zhang, S. Jiang, C. Sun, S. Song, Regulation of d-band centers in localized CdS homojunctions through facet control for improved photocatalytic water splitting, Angew. Chemie Int. Ed. 62 (2023) e202307808.

[11] H. Fu, Q. Zhang, Y. Liu, Z. Zheng, H. Cheng, B. Huang, P. Wang, Photocatalytic Overall Water Splitting with a Solar-to-Hydrogen Conversion Efficiency Exceeding 2% through Halide Perovskite, Angew. Chemie. 136 (2024) e202411016.

[12] X. Chen, J. Wang, Y. Chai, Z. Zhang, Y. Zhu, Efficient photocatalytic overall water splitting induced by the giant internal electric field of ag-C3N4/rGO/PDIP Z-scheme heterojunction, Adv. Mater. 33 (2021) 2007479.

[13] Y. Qi, B. Zhang, G. Zhang, Z. Zheng, T. Xie, S. Chen, G. Ma, C. Li, K. Domen, F. Zhang, Efficient overall water splitting of a suspended photocatalyst boosted by metal-support interaction, Joule. 8 (2024) 193–203.

[14] Y. Qi, Y. Zhao, Y. Gao, D. Li, Z. Li, F. Zhang, C. Li, Redox-based visible-light-driven Z-scheme overall water splitting with apparent quantum efficiency exceeding 10%, Joule. 2 (2018) 2393–2402.

[15] Z. Wang, Y. Inoue, T. Hisatomi, R. Ishikawa, Q. Wang, T. Takata, S. Chen, N. Shibata, Y. Ikuhara, K. Domen, Overall water splitting by Ta3N5 nanorod single crystals grown on the edges of KTaO3 particles, Nat. Catal. 1 (2018) 756–763.

[16] Y. Qi, J.W. Zhang, Y. Kong, Y. Zhao, S.S. Chen, D. Li, W. Liu, Y.F. Chen, T.F. Xie, J.Y. Cui, Unraveling of cocatalysts photodeposited selectively on facets of BiVO4 to boost solar water splitting, Nat. Commun. 13 (1)(2022) 484, (n.d.).

[17] L. Liu, S. Du, X. Guo, Y. Xiao, Z. Yin, N. Yang, Y. Bao, X. Zhu, S. Jin, Z. Feng, Water-stable nickel metal–organic framework nanobelts for cocatalyst-free photocatalytic water splitting to produce hydrogen, J. Am. Chem. Soc. 144 (2022) 2747–2754.

[18] H. Fu, Y. Wu, Y. Guo, T. Sakurai, Q. Zhang, Y. Liu, Z. Zheng, H. Cheng, Z. Wang, B. Huang, A scalable solar-driven photocatalytic system for separated H2 and O2 production from water, Nat. Commun. 16 (2025) 990.

[19] B. Kakavandi, M. Moradi, F. Hasanvandian, A. Bahadoran, E. Mohebolkhames, M. Golshan, S. Ganachari, T.M. Aminabhavi, Visible light-assisted S-scheme p-and n-type semiconductors anchored onto graphene for increased photocatalytic H2 production via water splitting, Chem. Eng. J. 487 (2024) 150399.